IEEE Access
Multidisciplinary | Rapid Review | Open Access Journal

Received March 5, 2021, accepted March 25, 2021, date of publication April 8, 2021, date of current version April 26, 2021.

Digital Object Identifier 10.1109/ACCESS.2021.3071486

Effective Conductivity of Additive-Manufactured Metals for Microwave Feed Components

RICHARD G. EDWARDS[1,2], (Member, IEEE), CRAIG M. NORTON[1], JARED E. CAMPBELL[1], AND DAVID SCHURIG[2], (Member, IEEE)

[1]L3Harris Technologies, Salt Lake City, UT 84116, USA
[2]Electrical and Computer Engineering Department, The University of Utah, Salt Lake City, UT 84112, USA

Corresponding author: Richard G. Edwards (richard.g.edwards@l3harris.com)

This work was supported in part by the L3 Harris Technologies.

ABSTRACT This paper characterizes the effective conductivity of lossy metal materials fabricated with additive manufacturing processes at microwave frequencies using a resonant cavity approach. Specifically addressed is the powder bed fusion additive manufacturing process utilizing AlSi10Mg material at Ku-band. The details of the procedure for converting device parameters that characterize the resonant cavity to material properties are given. Trade-offs between the precision of the conductivity and the quality factor of the cavity are discussed relevant to the design of the cavity. A best-fit matching procedure is made between the measured response of the manufactured cavities and the simulated results. The conductivity with statistical deviation for various fabricated cavities from different vendors is reported. Examples of various designs of fabricated prototype waveguide feed components are presented. The predicted and measured performance of each component is compared, validating the process.

INDEX TERMS 3D printing, additive manufacturing, attenuation, direct metal laser sintering, diplexer, filter, insertion loss, microwave, ortho-mode junction, powder bed fusion, selective laser melting, surface roughness, waveguide.

I. INTRODUCTION

The term additive manufacturing (AM) includes many processes that use many different types of base materials. The relatively recent development of additive manufacturing techniques in metal has enabled the design and manufacture of high performance antenna waveguide feed components at microwave frequencies [1], [2]. Additive manufacturing processes allow for the fabrication of structures that are very difficult if not impossible to build by other means. Examples of such components include: shaped sub-reflectors, waveguide feeds, ortho-mode junctions, polarizers, filters, diplexers, couplers, etc [3]–[8].

One major advantage of the additive manufacturing processes is the ability to create monolithic structures in contrast to assembling multiple parts. Such structures advantageously lack seams and joints, since even the smallest gap, at microwave frequencies, can disrupt or alter the flow of current. Current disruption can result in reflections, or the creation of localized, high-field intensities. High fields can lead to the increased likelihood of arcing at high power levels and conducive environmental conditions. Additionally, monolithic structures can be fabricated at a reduced cost, since the part count and assembly time are minimized.

Common techniques for the build of metal parts include casting and selective laser melting (SLM). Casting is a well-known process, although printing the mandrel with additive manufacturing techniques is relatively new. In this paper we focus on selective laser melting. In the literature selective laser melting is also known as direct metal laser sintering (DMLS) or powder bed fusion (PBF).

A non-comprehensive list of base metal materials utilized in the selective laser melting process includes copper, aluminum, gold, stainless steel, tool steel, cobalt chrome, titanium and tungsten, with many more being developed. Of interest for microwave applications are aluminum, copper and gold because of the high electrical conductivity at microwave frequencies. Aluminum is of special interest for antenna feed components because of its low density, and good thermal and electrical conductivity. It should be noted that many base

The associate editor coordinating the review of this manuscript and approving it for publication was Tutku Karacolak.

materials are alloys designed to yield desired properties of the finished part, such as surface finish and density. One common alloy is aluminum-silicon-magnesium (AlSi10Mg), which will be the primary material investigated in this paper.

Of major interest in the design of waveguide components is the amount of power loss through the device [9], [10]. For air-filled (no-dielectric) metal parts the loss is inversely related to the electrical conductivity. The conductivity is of special interest to the device designer, since this single parameter is used to characterize lossy metal conductors in the analysis tools used to predict the performance of microwave components.

There are various techniques for characterizing the loss through microwave devices. Generally the techniques fall into two main categories: those that utilize non-resonant structures such as transmission lines and waveguides [11], and those that utilize resonant structures. The latter often quantify loss through the quality factor (Q), (though fitting the actual resonant response can offer advantages as discussed below) [12]. Cavity techniques are of particular interest since they provide a small form factor and high sensitivity to conductivity [13].

Our approach is similar to that of reference [14], though we take an intermediate approach, using a more strongly coupled cavity (with low quality factor), which gives a significant response over a wider range of frequencies. Reference [15] uses a strongly coupled cavity, however only provides an approximate estimation of the effective conductivity and lacks the statistical analysis quantifying variation. We apply this approach specifically to parts produced via SLM processing of AlSi10Mg, and provide theory and results for the extraction of conductivity from measurements at frequencies near 15 GHz. A rigorous determination of the conductivity uncertainty is also included. Our analysis separates the large-scale geometric variations (i.e. not the surface roughness) from the material properties, and demonstrates that if this is not done then erroneous results will be obtained.

Section II gives the details of the design of the resonant cavity, along with the methods used to predict the conductivity from the response of the cavity as characterized by generalized network scattering parameters. Results are given in Section III, including predicted conductivity and variances of various sample cavities, manufactured by multiple vendors. Also included, is a validation of our methods using the derived conductivity in the simulation of various microwave components. The measured response of these fabricated parts are compared to simulation results, with good agreement, specifically highlighting the loss through the parts. Finally, conclusions and future work are provided in Section IV.

II. METHOD FOR DETERMINING CONDUCTIVITY

Our approach is based on the well-known surface impedance model with the following assumptions [16]:

- The curvature of the wall is much larger than the skin depth δ.
- The conduction current in the wall is much larger than the displacement current.
- The field relationships at the waveguide walls are given by a plane-wave analysis.

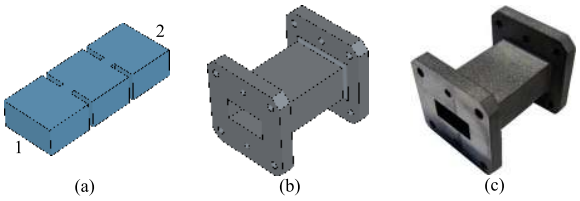

FIGURE 1. Illustration of the (a) electrical model with port designations, (b) mechanical model, and (c) manufactured prototype of the rectangular resonant cavity.

The surface impedance at the wall may be expressed as

$$Z_s = \sqrt{\frac{j\omega\mu}{\sigma + j\omega\varepsilon}} \approx \frac{1+j}{\sigma\delta} \tag{1}$$

with

$$\delta = \sqrt{\frac{2}{\omega\mu\sigma}} \tag{2}$$

where ω is the radian frequency, μ is the permeability, ε is the permittivity of the material and δ is the skin depth.

Because of the use of the surface impedance model, the loss is a function of many variables, both intrinsic and extrinsic. A non-comprehensive list includes frequency, surface finish, layer print resolution, build orientation, laser spot size, laser intensity, base material chemical composition, impurities in the base material, post processing, cleaning, etc. There is no attempt to separate the effect of each of these, rather we quantify the conductivity from one specific build process readily available from multiple manufacturers.

It should be noted that the theory is general and can be applied to any AM process capable of building the resonant cavity geometry with a base material that is electrically conductive. This is accomplished by designing and manufacturing resonant cavities (see Fig. 1) with resonance at the frequency of interest.

The advantage of this technique is that the loss near resonance is sensitive to changes in the conductivity, allowing for better resolution of the value. This is demonstrated in Fig. 2, which shows a typical example of loss through a microwave cavity with varying values of conductivity. The results were obtained by using a lossy mode-matching technique described in more detail in Section II-B and verified with the finite element method. The loss (L) is defined for an n-port network characterized by scattering parameters to be

$$L_j = -10\log\left(\sum_{i=1}^{n} |S_{i,j}|^2\right) \tag{3}$$

given power input into the j-th port. This is an expression of the conservation of energy of a closed system.

In contrast, the loss through a non-resonant structure such as a transmission line or waveguide is small, making it more

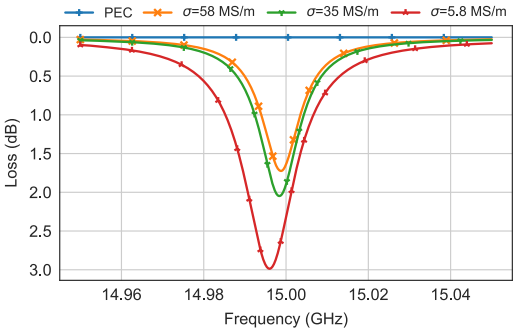

FIGURE 2. Loss through a resonant cavity as a function of electrical conductivity where the loss is defined from the 2-port network scattering parameters to be $L = -10\log(|S_{1,1}|^2 + |S_{2,1}|^2)$.

difficult to resolve the conductivity, although it is valid over a broad range of frequencies. The disadvantage with the resonance technique is that the conductivity is only valid over a relatively small range of frequencies. Our approach compromises between the two extremes, where we use a lower quality factor (high coupling) that allows for enough sensitivity to resolve the parameter of interest (in our case conductivity).

A resonant microwave cavity can be characterized by a resonant frequency (f_c) and a quality factor (Q). The quality factor is a measure of the lifetime of free oscillations. An energy based definition of the quality factor is given as 2π times the ratio of the mean stored energy over the dissipated power [17]. Another definition of the quality factor is derived from the frequency derivative of the input impedance and can be expressed as $Q = f_c/\Delta f$ where f_c is the center frequency and Δf is the 3-dB bandwidth [16], [17]. From Foster's reactance theorem, these two definitions generally yield distinct results, however they asymptotically approach each other as loss becomes increasingly small [18], [19]. The energy based definition is well defined, where the definition based on bandwidth is only a good approximation given low loss and small coupling, which uses only three frequency points to estimate the quality factor. Therefore, given the relatively high coupling values of the cavity and potentially high loss of the materials of interest, we are required to analyze the response over a broad frequency band sampled at many points, with an analysis technique that accurately accounts for the dissipated energy.

In order to determine the conductivity, we compare the results from a simulation based on a simple parameterized model with the measured results of a manufactured cavity. This comparison is reduced to a value whose magnitude is related to the quality of the match between the measured and simulated results. We then use optimization algorithms to adjust the model parameters until a best match is obtained that minimizes the squared error residuals between the simulated and measured results.

A. MODEL

The model used (see Fig. 3) was chosen to provide the desired response while minimizing the number of parameters

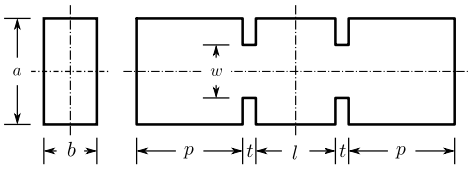

FIGURE 3. Parametric model of a simplified rectangular cavity.

necessary to describe the geometry. This was accomplished by reusing parameters from symmetric features and utilizing planar symmetries in the rectangular coordinate system.

The geometric parameters of the cavity were designed so that resulting external quality factor (ignoring wall loss) is approximately 1500 at a center resonant frequency of 15 GHz. The relatively large coupling, resulting in a smaller quality factor, is mainly controlled by increasing the iris width (w) of the cavity. A larger iris width, generally makes the manufacturing of the cavity with additive manufacturing methods more practical, providing greater access to the inside of the cavity. For example, the SLM process leaves powder in the voids of the cavity which needs to be removed. Other manufacturing methods may also require the removal of temporary supports.

Large quality factors result in small relative bandwidths leading to increased sensitivity with respect to the model parameters. Therefore, there is a design compromise between the resolution of the parameter value of interest (in our case conductivity) and the ability to practically manufacture, analyze and measure the response of the such structures.

B. ANALYSIS

The analysis of the parametric model can be performed with a number of numerical techniques [20] given that they yield a generalized scattering matrix that includes loss. The method used in our analysis is based on the mode-matching technique [21], [22] with the inclusion of conductor loss on the waveguide walls [23]. The advantage of such a method over more conventional, general-purpose electromagnetic solvers is the speed at which the calculations can be executed. A fast computational algorithm is attractive due to the large number of iterations required by the least-squares fit procedure, although it is not necessary. Most general purpose solvers are mesh based, and for resonant structures the mesh needs to be fine for accurate results, leading to relatively long run times. In contrast, the mode-matching models are semi-analytic, resulting in accurate and fast simulations, thus making the fit procedure more time efficient. A comparison of the results between the lossy mode-matching technique and a commercially available mesh-based simulation tool is shown in Fig. 4, demonstrating excellent agreement between the two methods.

The results compare well with only a slight frequency shift between the methods. This can be influenced by the mesh size in the general full-wave solver and also by the number of expansion-modes used in the mode-matching technique. It is noted that the results compare particularly well for the case

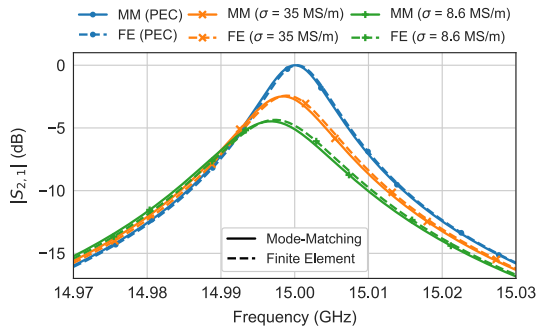

FIGURE 4. Comparison of the predicted magnitude of $|S_{2,1}|$ of a two-port resonant cavity simulated with a lossy mode-matching technique (MM) and a mesh-based finite-element electromagnetic solver (FE) at various values of conductivity.

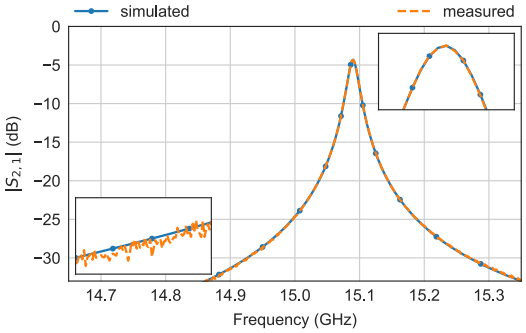

FIGURE 5. Typical measured and simulated results after optimization of a resonant cavity utilizing a cost function that minimized the difference in the square of the magnitude of the transmission coefficients over frequency. Also shown is a detail plot at the peak of resonance and a range that illustrates the fit of the simulated and noisy measured data.

with no loss, showing identical magnitude and only a slight frequency shift. Discrepancies observed in the magnitude of $S_{2,1}$ may be a result of the approximations used in the numerical calculation of the complex propagation constants in the mode-matching code [23]. In any case, convergence analysis of the scattering parameters should be carried out with the analysis tool of choice in order to guarantee accurate results.

C. MEASUREMENT

The experimental characterization of the prototype cavities was performed with a vector network analyzer and using a waveguide calibration kit. The latter ensured the measured magnitude and phase of the transmission and reflection coefficients had a known reference plane at the flanges of the cavity. This allows for a direct comparison with the generalized scattering matrix of the simulated results.

Errors that can degrade the accuracy of the results include systematic and non-systematic errors. Examples of systematic errors, include calibration errors whereas non-systematic errors are quantified as noise. An example of the measured response of a cavity is shown in Fig. 5.

D. OPTIMIZATION

There are many ways to calculate the error that quantifies the quality of the match between the measured and simulated results. The technique that was used in this study is based on the root-mean-squared difference between the magnitude of the measured and simulated transmission coefficients such that

$$\varepsilon = \frac{1}{bw}\sqrt{\int_{f_{min}}^{f_{max}} \left(|T_{meas}(f)| - |T_{sim}(f)|\right)^2 df} \qquad (4)$$

where ε is the error or residual, $bw = f_{max} - f_{min}$, and f_{min} and f_{max} are the limits of the frequency band of interest. The parameters T_{meas} and T_{sim} are the complex transmission coefficients of the measured and simulated results, respectively. The difference in the magnitude of the transmission coefficients (neglecting phase) was found to be sufficient in order to obtain a quality fit.

There are various optimization techniques to minimize the error. Ideally, the optimizer would be one that does not rely on the gradient of the error function but only on the error function itself. We found it advantageous to provide manually chosen initial guesses before starting the optimization, especially since a local optimizer is utilized.

Illustrated in Fig. 5 is a typical comparison between measured and simulated results after optimization. The measured and simulated results agree very well, indicating that our model sufficiently describes the physical response of the resonant cavity. The magnitude of the errors appear to be within the noise of the measured response.

III. RESULTS

The test parts were produced by two different 3D printing vendors with a build quantity of three cavities from each. Referring to Fig. 3, we observed a strong correlation between the resonant frequency of the cavity, the width of the waveguide, a, and the length of the cavity, l. We also found a strong correlation between the magnitude of the transmission at resonance and the conductivity, σ, and the waveguide height, b. Because of the correlation between parameters, in order to calculate the conductivity based on the measured results, we measured the physical dimensions a and b and fixed them to constants in the optimization. We then minimized the error as a function of the variables σ, w, t and l until a best match was found. The parameters a and b were then varied within a specified tolerance, and the minimization process was repeated. The uncertainty for a and b was chosen to be ± 0.127 mm, which was based on the manufacturer's claimed accuracy and our own independent measurements. We independently varied the parameters a and b in the analysis, choosing 5 different points for each, for a total of $n = 25$ different samples evenly spaced on a 5×5 grid (see Fig. 6). This process was then repeated for each of the six cavities. The conductivity for each of the 25 configurations was statistically analyzed.

The mean conductivity and the uncertainty of the mean for each cavity is summarized in Table 1. The uncertainty of the mean is given as $s/\sqrt{n}$ where s is the standard deviation and

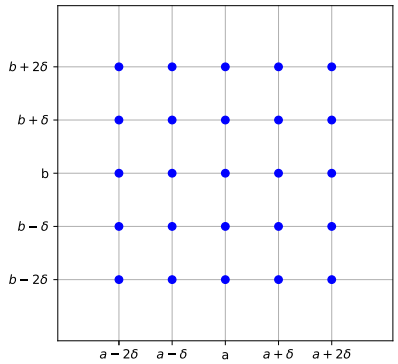

FIGURE 6. The nominal waveguide width a and the waveguide height b were measured for each cavity and then sampled on a 5 × 5 grid over the total prescribed tolerance with $\delta = 0.0635$ mm.

TABLE 1. Effective conductivity (MS/m).

	Vendor 1	Vendor 2
Cavity 1	9.071 ± 0.023	7.902 ± 0.020
Cavity 2	8.804 ± 0.022	8.908 ± 0.023
Cavity 3	8.785 ± 0.022	8.418 ± 0.021
Vendor 1-2	Vendor 1	Vendor 2
8.65 ± 0.40	8.89 ± 0.17	8.41 ± 0.42

n is the number of samples [24]. We note that this uncertainty is substantially smaller than differences in the conductivity observed between different cavities. Thus, our process is able to observe variations between identically specified cavities from different vendors or even the same vendor's process variation.

We also report in Table 1 the mean conductivity and the standard deviation for each vendor individually and for both vendors together. This demonstrates the differences in the results from the individual vendors. If one wishes to work with a single vendor, then it is likely the uncertainty of the results can be minimized, given that the process parameters are controlled more tightly.

In order to verify the presented results, we use the resultant conductivity values in Table 1 to design and predict the loss through various microwave components. Each of these components was manufactured and then measured and finally compared against predicted values.

A. KU-BAND DIPLEXER

Our first example demonstrates the design of a Ku-band diplexer whose structure is shown in Fig. 7. A diplexer is a 3-port device that separates two different frequency bands in a communications system. It is composed of a combiner/splitter and two filters. The filters in this design are band-pass coupled resonant cavity filters. The filters are folded in order to minimize the overall structure length. The high Q-value of this structure makes it sensitive to dimensional variations. The prototype diplexer in Fig. 7 (c) was manufactured using Vendor 2 in Table 1. Therefore, a conductivity of $\sigma = 8.41$ MS/m was used to simulate the electrical model in Fig. 7 (a).

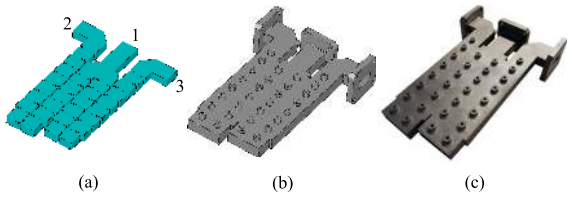

FIGURE 7. Illustration of the (a) electrical model with port designations, (b) mechanical model, and (c) manufactured prototype of a Ku-band diplexer. Even though provisions for tuning screws are illustrated in (b) and (c), they were not utilized in this work.

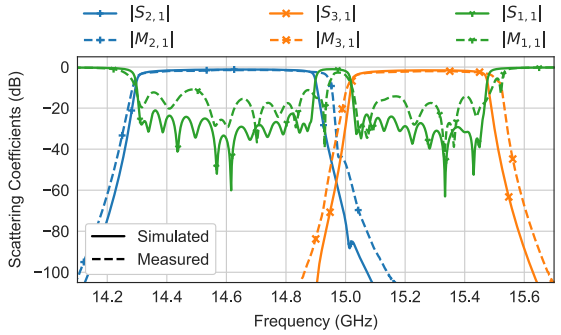

FIGURE 8. A comparison of the simulated ($S_{i,j}$) and measured ($M_{i,j}$) modal scattering coefficients of the Ku-band diplexer structure. A conductivity of $\sigma = 8.41$ MS/m was used in the simulation.

A comparison of the simulated and measured results are shown in Fig. 8. As can be observed, the pass-band bandwidths for the measured results are slightly wider than the predicted results. The most likely cause of this is the geometric uncertainty of the iris widths w. This can be remedied by making small adjustments to the model and iterating in the build process until the desired results are achieved [9].

Also observed is a slight difference in the magnitude of the reflection coefficient $|S_{1,1}|$ between the measured and predicted results. The sensitivity of the resonance is influenced by the lengths l of the cavities, and length variations are most likely the cause of the difference. Given a sufficiently small initial return loss (>10 dB), then the reflection coefficient can be minimized with the aid of tuning screws. Illustrated in Fig. 7 (b) and (c) are the provisions for the installation of tuning screws, however they were not utilized in this work. The focus of this work is to predict the loss and characteristics of the device based on the manufacturing process by itself and not with the aid of adjustments made by tuning. The tuning is considered a secondary process to be avoided if possible.

The loss analysis is shown in Fig. 9 where loss is defined with respect to the generalized scattering matrix elements as $\text{Loss(dB)} = -10\log(|S_{1,3}|^2 + |S_{2,3}|^2 + |S_{3,3}|^2)$. As can be observed, there is good agreement between predicted and measured results. Also shown is the erroneous result one would achieve if applying the conductivity of pure aluminum ($\sigma \approx 35$ MS/m) to the simulation.

B. LOW-PASS FILTER

Our second example includes the design and prototyping of a 2-port low-pass filter at Ka-band whose geometry is shown in Fig. 10. The prototype filter in Fig. 10(c) was manufactured

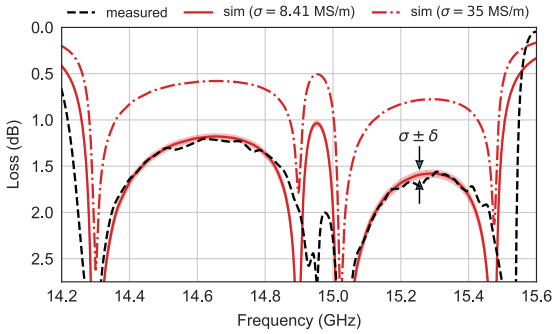

FIGURE 9. Illustration of the Ku-band diplexer loss analysis with the loss being defined as Loss $= -10\log(|S_{1,3}|^2 + |S_{2,3}|^2 + |S_{3,3}|^2)$. Shown is a comparison between the measured and simulated results with the conductivity calculated from the resonant cavity technique with $\sigma = 8.41$ MS/m. The widening of the line around the nominal indicates the predicted loss values for a conductivity spanning a range of plus or minus one standard deviation (δ). Also shown is the simulated result using a reference conductivity of $\sigma = 35$ MS/m, which is approximately the conductivity of pure aluminum.

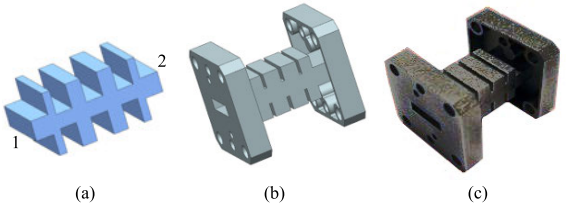

FIGURE 10. Illustration of the (a) electrical model, (b) mechanical model, and (c) manufactured prototype of a Ka-band low-pass filter.

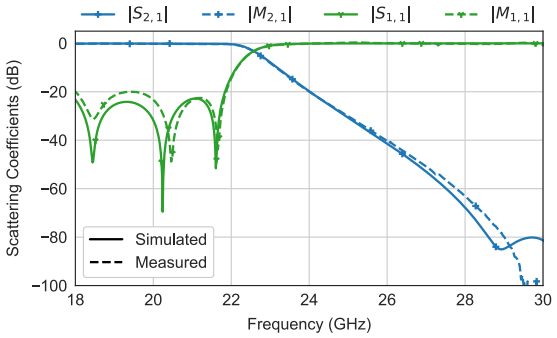

FIGURE 11. A comparison of the simulated ($S_{i,j}$) and measured ($M_{i,j}$) modal scattering coefficients of the Ka-band low-pass filter structure. A conductivity of $\sigma = 8.65$ MS/m was used in the simulation.

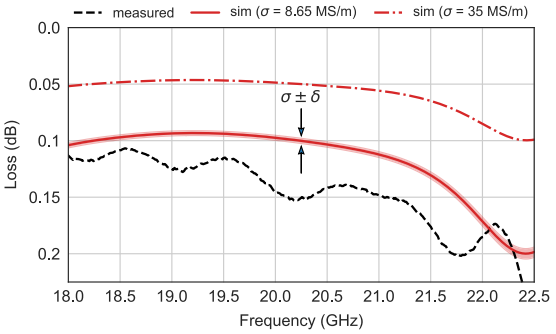

FIGURE 12. Illustration of the Ka-band low-pass filter loss analysis with the loss being defined as Loss $= -10\log(|S_{1,1}|^2 + |S_{2,1}|^2)$. Shown is a comparison between the measured and simulated results with the conductivity calculated from the resonant cavity technique with $\sigma = 8.65$ MS/m. The widening of the line around the nominal indicates the predicted loss values for a conductivity spanning a range of plus or minus one standard deviation (δ). Also shown is the simulated result using a reference conductivity of $\sigma = 35$ MS/m, which is approximately the conductivity of pure aluminum.

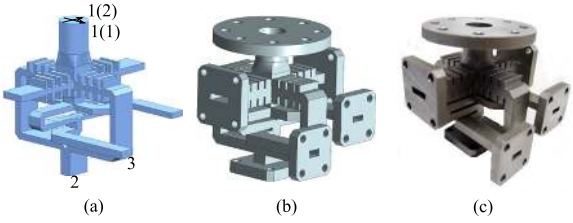

FIGURE 13. Illustration of the (a) electrical model with port and mode (in parentheses) designations, (b) mechanical model, and (c) manufactured prototype of an ortho-mode diplexer structure.

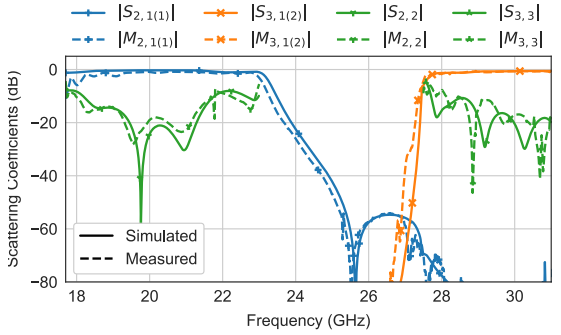

FIGURE 14. A comparison of the simulated ($S_{i,j}$) and measured ($M_{i,j}$) modal scattering coefficients of the ortho-mode diplexer structure. A conductivity of $\sigma = 8.65$ MS/m was used in the simulation.

using a different vendor from either vendor used to manufacture the resonant cavities in Table 1. The frequency of operation is also higher than the resonant frequency of the cavities used to determine the conductivity. Therefore, we chose an average conductivity of $\sigma = 8.65$ MS/m (see Table 1) in order to simulate the electrical model in Fig. 10(a), which is a reasonable choice since it is unknown for this vendor.

The measured and predicted results are shown in Fig. 11, which are seen to have good agreement for the transmission and reflection coefficients. In this case, even though the frequencies of interest are higher than in the previous example, the filter has a lower Q-value, making it less sensitive to dimensional variations and thus yielding good agreement between predicted and measured results.

The pass-band loss analysis is shown in Fig. 12, where the loss is defined as Loss $= -10\log(|S_{1,1}|^2 + |S_{2,1}|^2)$. Given the limited knowledge of the effect of the process parameters on the conductivity at the frequencies of interest, there is still good agreement between measured and simulated results. As observed, the simulated results are slightly optimistic. As previously discussed, this can be due to many different factors which are dependent on the process parameters of a given vendor. One of these is surface roughness, which creates frequency-dependent loss [25].

C. ORTHO-MODE DIPLEXER

Our final example incorporates the design of the low-pass filter from the previous example and a high pass-filter (cutoff

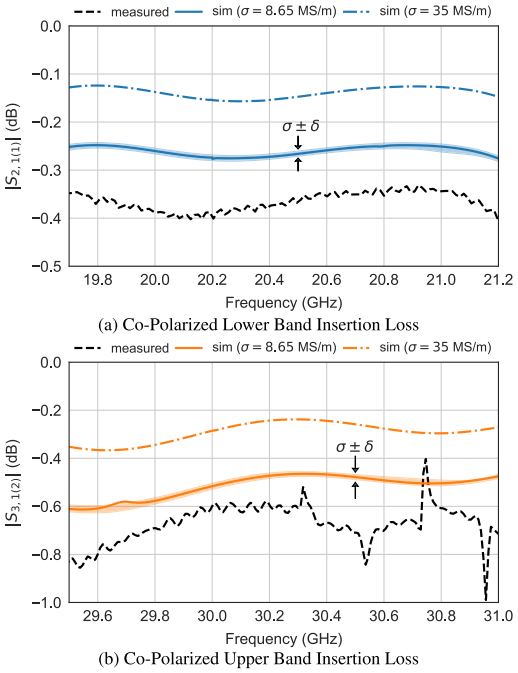

FIGURE 15. Comparison of simulated and measured results of the co-polarized pass-band transmission coefficients through the ortho-mode diplexer. Shown is a comparison between the measured and simulated results with the conductivity calculated from the resonant cavity technique with $\sigma = 8.65$ MS/m. The widening of the line around the nominal indicates the predicted loss values for a conductivity spanning a range of plus or minus one standard deviation (δ). Also shown is the simulated result using a reference conductivity of $\sigma = 35$ MS/m, which is approximately the conductivity of pure aluminum.

waveguide) with an ortho-mode turnstile junction resulting in a geometrically complex structure shown in Fig. 13. Similar structures were investigated in [26]–[28]. The manufacture of such a structure without seams would be very difficult using conventional manufacturing techniques. The device is a multiple-port device where the common port is a circular waveguide supporting two fundamental degenerate orthogonal waveguide modes. These modes are designated in Fig. 13(a) as 1(1) and 1(2) and constitute independent solutions in the generalized scattering matrix. For the co-polarized modes, the behavior is similar to that of a diplexer, and for this reason this device has been given the name of an ortho-mode diplexer (OMD), as it combines the function of a diplexer and an ortho-mode junction in a compact form factor. In the literature, the structure is also known as a dual-polarization diplexer.

The same process parameters from the same vendor used to manufacture the low-pass filter in the previous example were utilized for this case. Since our interest is in the pass-band insertion loss, we show results for only the co-polarized transmission coefficients and do not show the cross-polarized components. The ports not labeled in Fig. 13 (a) should be considered loaded with an absorber.

The predicted and measured results are shown in Fig. 14 with good agreement. The transmission coefficients in the lower and upper pass-bands are shown in Fig. 15 (a) and (b), respectively. Similarly to the previous low-pass filter example, the simulated loss is slightly optimistic for the same reasons given previously. It should be noted that in this example the conductivity model was extended to higher frequencies ($\approx$ 30 GHz) and still demonstrates good agreement.

IV. CONCLUSION

In this work we have developed the tools and demonstrated a procedure to calculate the conductivity of a lossy metal using a resonant cavity approach. We have provided statistical results (mean and deviation) of the accuracy of the technique. We have specifically applied this approach to the prediction of the conductivity at Ku-band frequencies of components fabricated with the selective laser melting additive manufacturing process with the AlSi10Mg material.

It has been shown that the conductivity of AlSi10Mg is significantly lower than that of pure aluminum at microwave frequencies. Acceptable results for a given application must be evaluated on a case-by-case basis.

These results were then applied to the design and fabrication of example antenna feed components including a Ku-band diplexer, a Ka-band low-pass filter, and a more complex Ka-band ortho-mode diplexer. For each example, measured and predicted results were compared, and the results showed good agreement.

Future work includes extending the analysis to include other materials and processes and extended frequency bands. The frequency-dependent effect of surface roughness for a given process is also currently being investigated. Future work also includes the development of new materials and processes specifically designed for microwave feed components. Increased conductivity and reduced surface roughness will enable higher performance while maintaining the advantages of monolithic structures. It is envisioned that as this process matures and similar new processes are developed, novel high-performance and functional microwave components will be realized.

REFERENCES

[1] F. Calignano, D. Manfredi, E. P. Ambrosio, S. Biamino, M. Lombardi, E. Atzeni, A. Salmi, P. Minetola, L. Iuliano, and P. Fino, "Overview on additive manufacturing technologies," *Proc. IEEE*, vol. 105, no. 4, pp. 593–612, Apr. 2017, doi: 10.1109/JPROC.2016.2625098.

[2] A. Gomez-Torrent, F. Teberio, A. Martinez, J. M. Percaz, I. Arnedo, I. Maestrojuan, I. Arregui, G. Crespo, T. Lopetegi, M. A. G. Laso, and J. Teniente, "A study of the additive manufacturing technology for RF/microwave components," in *Proc. 11th Eur. Conf. Antennas Propag. (EUCAP)*, Mar. 2017, pp. 567–571, doi: 10.23919/EuCAP.2017.7928732.

[3] D. Shamvedi, O. J. McCarthy, E. O'Donoghue, P. O'Leary, and R. Raghavendra, "3D metal printed monocone antenna with an integrated feed," in *Proc. 47th Eur. Microw. Conf. (EuMC)*, Oct. 2017, pp. 168–171, doi: 10.23919/EuMC.2017.8230826.

[4] M. Hanqing, W. Dong, S. Junfeng, and T. Jiang, "A wideband 45 degree polarized electrical scanning antenna array manufactured by 3D printing with metals," in *Proc. CIE Int. Conf. Radar (RADAR)*, Oct. 2016, pp. 1–3, doi: 10.1109/RADAR.2016.8059418.

[5] Z. Shi-Gang, H. Guan-Long, and C. Tan-Huat, "Dual circular polarized array with metal 3D-printing," in *Proc. IEEE 5th Asia–Pacific Conf. Antennas Propag. (APCAP)*, Jul. 2016, pp. 43–44, doi: 10.1109/APCAP.2016.7843090.

[6] T. H. Chio, G. L. Huang, S. G. Zhou, and W. Y. Lim, "A 3D-printed compact dual-circularly polarized corrugated horn with integrated septum polarizer," in *Proc. Int. Symp. Antennas Propag. (ISAP)*, Oct. 2016, pp. 272–273.

[7] A. Vosoogh, P.-S. Kildal, V. Vassilev, A. U. Zaman, and S. Carlsson, "E-band 3-D metal printed wideband planar horn array antenna," in *Proc. Int. Symp. Antennas Propag. (ISAP)*, Oct. 2016, pp. 304–305.
[8] J. A. Gordon, D. R. Novotny, M. H. Francis, R. C. Wittmann, M. L. Butler, A. E. Curtin, J. R. Guerrieri, L. Periasamy, and A. J. Gasiewski, "An all-metal, 3-D-printed CubeSat feed horn: An assessment of performance conducted at 118.7503 GHz using a robotic antenna range," *IEEE Antennas Propag. Mag.*, vol. 59, no. 2, pp. 96–102, Apr. 2017, doi: 10.1109/MAP.2017.2655574.
[9] O. A. Peverini, G. Addamo, M. Lumia, G. Virone, F. Calignano, M. Lorusso, and D. Manfredi, "Additive manufacturing of Ku/K-band waveguide filters: A comparative analysis among selective-laser melting and stereo-lithography," *IET Microw., Antennas Propag.*, vol. 11, no. 14, pp. 1936–1942, Nov. 2017, doi: 10.1049/iet-map.2017.0151.
[10] G. Addamo, O. A. Peverini, M. Lumia, G. Virone, R. Tascone, F. Calignano, and D. Manfredi, "Experimental research activity on additive manufacturing of microwave passive waveguide components," in *Proc. 47th Eur. Microw. Conf. (EuMC)*, Oct. 2017, pp. 496–499, doi: 10.23919/EuMC.2017.8230898.
[11] M. Hollenbeck, K. Wamick, C. Cathey, J. Opra, and R. Smith, "Selective laser melting aluminum waveguide attenuation at K-band," in *IEEE MTT-S Int. Microw. Symp. Dig.*, Jun. 2017, pp. 45–47, doi: 10.1109/MWSYM.2017.8058605.
[12] S.-H. Chao, "Measurements of microwave conductivity and dielectric constant by the cavity perturbation method and their errors," *IEEE Trans. Microw. Theory Techn.*, vol. MTT-33, no. 6, pp. 519–526, Jun. 1985, doi: 10.1109/TMTT.1985.1133108.
[13] R. Królak and G. Fischerauer, "Q-factor estimation from the return loss of low-Q microwave resonators," *IEEE Trans. Microw. Theory Techn.*, vol. 64, no. 11, pp. 3797–3806, Sep. 2016, doi: 10.1109/TMTT.2016.2605673.
[14] T. Jungkunz and G. Fischerauer, "Resonance parameter estimation for low-Q microwave cavities," in *Proc. Int. Multi-Conf. Syst., Signals Devices*, Mar. 2012, pp. 1–6, doi: 10.1109/SSD.2012.6198094.
[15] O. A. Peverini, M. Lumia, G. Addamo, F. Calignano, G. Virone, E. P. Ambrosio, D. Manfredi, and R. Tascone, "Integration of RF functionalities in microwave waveguide components through 3D metal printing," in *IEEE MTT-S Int. Microw. Symp. Dig.*, Jun. 2017, pp. 48–51, doi: 10.1109/MWSYM.2017.8058615.
[16] C. C. Johnson, *Field and Wave Electrodynamics*. New York, NY, USA: McGraw-Hill, 1965.
[17] R. E. Collin, *Foundations for Microwave Engineering*. Hoboken, NJ, USA: Wiley, 2007.
[18] M. Capek, L. Jelinek, and G. A. E. Vandenbosch, "Stored electromagnetic energy and quality factor of radiating structures," *Proc. Roy. Soc. A, Math., Phys. Eng. Sci.*, vol. 472, no. 2188, Apr. 2016, Art. no. 20150870.
[19] R. M. Foster, "A reactance theorem," *Bell Syst. Tech. J.*, vol. 3, no. 2, pp. 259–267, Apr. 1924.
[20] C. Su, H. Ke, and T. Hubing, "Overview of electromagnetic modeling software," in *Proc. 25th Int. Rev. Prog. Appl. Comput. Electromagn.*, Mar. 2009, pp. 736–741.
[21] J. Uher and J. Bornemann, *Waveguide Components for Antenna Feed Systems: Theory and CAD*. Boston, MA, USA: Artech House, 1993, p. 476.
[22] G. Conciauro, M. Guglielmi, and R. Sorrentino, *Advanced Modal Analysis*, 1st ed. Chichester, U.K.: Wiley, 2000, p. 356.
[23] J. D. Jackson, *Classical Electrodynamics*, 3rd ed. New York, NY, USA: Wiley, 1998, p. 832.
[24] Wikipedia Contributors. (2018). *Standard Error—Wikipedia, the Free Encyclopedia*. Accessed: Apr. 26, 2018. [Online]. Available: https://en.wikipedia.org/w/index.php?title=Standard_error&oldid=836651912
[25] G. Gold and K. Helmreich, "A physical surface roughness model and its applications," *IEEE Trans. Microw. Theory Techn.*, vol. 65, no. 10, pp. 3720–3732, Oct. 2017, doi: 10.1109/TMTT.2017.2695192.
[26] A. Bhutani, J. Schaefer, M. Pauli, S. Scherr, B. Goettel, M. Nierlich, and T. Zwick, "3D metal printed Ku/Ka band modified turnstile junction orthomode transducer," in *Proc. Asia–Pacific Microw. Conf. (APMC)*, Dec. 2016, pp. 1–4, doi: 10.1109/APMC.2016.7931276.
[27] J. R. Montejo-Garai, J. A. Ruiz-Cruz, C. A. Leal-evillano, and J. M. Rebollar, "Modelling of dual-polarisation diplexers based on enhanced multiport turnstile junctions," *IET Microw., Antennas Propag.*, vol. 7, no. 7, pp. 485–492, May 2013, doi: 10.1049/iet-map.2012.0424.
[28] H. Yukawa, Y. Ushijima, M. Abe, N. Yoneda, and M. Miyazaki, "A metal 3D-printed T-junction OMT with an offset stepped post," in *Proc. 47th Eur. Microw. Conf. (EuMC)*, Oct. 2017, pp. 444–447, doi: 10.23919/EuMC.2017.8230885.

RICHARD G. EDWARDS (Member, IEEE) received the B.S. and M.E. degrees from the Electrical and Computer Engineering Department, The University of Utah, Salt Lake City, UT, USA, in 1999 and 2000, respectively. He is currently pursuing the Ph.D. degree in electrical engineering with The University of Utah.

Since 2000, he has been employed at L3Harris CSW, Salt Lake City, where he also works as a Research and Design Engineer developing antennas for state-of-the-art communication systems. His current research interests include the modeling and design of high-performance antenna systems and supporting components for mobile airborne platforms and the investigation of novel manufacturing techniques at microwave frequencies.

CRAIG M. NORTON received the B.S. and M.S. degrees from the Mechanical Engineering Department, The University of Utah, Salt Lake City, UT, USA, in 1996 and 2004, respectively.

Since 2004, he has been employed at L3Harris CSW, Salt Lake City, where he also works as a Design Engineer developing and analyzing mechanical aspects of antennas and other components of state-of-the-art communication systems. He has worked extensively in commercial aerospace and military technology. His current research interests include the utilization of various 3D printing technologies and novel manufacturing techniques to produce complex components.

JARED E. CAMPBELL received the B.S. degree from the Mechanical Engineering Department, The University of Utah, Salt Lake City, UT, USA, in 2002.

Since 2003, he has been employed at L3Harris CSW, Salt Lake City, where he also works as a Chief Engineer of the Hardware Engineering Group in which he coordinates research and development efforts in the areas of thermal management, additive manufacturing, and antenna development. His previous roles include a Mechanical Design Engineer, a Structural and Thermal Analyst, the Lead of the Active Mechanical Controls Group, and the Chief Technologist of Mechanical Engineering. His experience prior to CSW includes research at The University of Utah in the fields of computational and physical fluids dynamics. His current research interests are focused on maturation and transition of low-to-medium technology readiness level (TRL) technologies that demonstrate significant cost, size, weight and power (cSWaP) benefits. His variations on common additive manufacturing (AM) techniques, materials, and processing is an area of focus due to direct application to improve specialty RF components.

DAVID SCHURIG (Member, IEEE) received the B.S. degree in engineering physics from the University of California at Berkeley, Berkeley, CA, USA, and the Ph.D. degree in physics from the University of California at San Diego, La Jolla, CA, USA, in 2002.

He joined the Lawrence Berkeley Laboratory, Berkeley, where he was involved in laser ablation and photoacoustic spectroscopy. After enrolling in graduate school and performing many unpublished experiments, he submitted a theoretical thesis on negative index media, the perfect lens, and related structures. He was with Tristan Technologies, San Diego, CA, USA, where he designed and built cryogenically cooled superconducting quantum interference device-based instruments. He joined Duke University, Durham, NC, USA, where he was supported by the Intelligence Community Postdoctoral Fellowship Program. He was briefly an Associate Professor with the Electrical and Computer Engineering Department, North Carolina State University, Raleigh, NC, USA. He joined the Electrical and Computer Engineering Department, The University of Utah, Salt Lake City, UT, USA, in 2011.